Tracking in Detail the Synthesis of Cadmium Oxide from a Hydroxyl Gel Using Combinations of in Situ X-ray Absorption Fine Structure Spectroscopy, X-ray Diffraction, and Small-Angle X-ray Scattering

C. Alétru,[†] G. N. Greaves,*[,†] and G. Sankar[‡]

Department of Physics, University of Wales, Aberystwyth, SY23 3BZ, U.K., and The Royal Institution of Great Britain, 21 Albemarle Street, London, WX1 4BS, U.K.

Received: October 20, 1998; In Final Form: February 5, 1999

The synthesis of cadmium oxide from a gel of cadmium hydroxide has been followed in situ using unique combinations of X-ray diffraction (XRD), X-ray absorption fine structure (XAFS) spectroscopy, and small-angle X-ray scattering (SAXS). XRD and XAFS enable the crystallography, particle size, and local structure to be quantified as the hydroxyl gel converts into cadmium oxide around 182 °C. SAXS measures the evolving microstructure, with cadmium oxide growing dendritically in a fractal geometry, initially from rough nanoparticles. Major growth and densification takes place between 325 and 550 °C. The implications for characterizing the precipitation of cadmium oxide nanoparticles in zeolitic hosts are considered.

Introduction

Chemie douce techniques provide attractive energy efficient routes for synthesizing highly homogeneous and, in some cases, microporous materials. For instance, sol−gel techniques[1] involve solvent removal at comparatively low temperatures, which leaves materials highly dispersed and nanophasic,[2] while densification to form monophasic ceramics can often be achieved by subsequent treatment at temperatures scarcely half those employed in conventional sintering methods. Complex processes such as these involve substantial changes in phase and order both on the atomic and on the nanostructural scale, and detailed characterization necessitates the deployment of in situ structural probes to properly chart their various careers. In the early stages phases may be amorphous and/or nanocrystalline, which precludes standard X-ray diffraction (XRD) methods, requiring recourse to local structure spectroscopies such as X-ray absorption fine structure (XAFS) spectroscopy, and NMR.[3−5] Given a combination of phases altering with time and temperature or pressure, these will be projected onto an evolving microstructure, often best probed using small-angle X-ray scattering (SAXS).[6−8] Bringing X-ray techniques together in single experiments[9−12] has proved an extremely versatile approach for characterizing in situ sol−gel[13] and other solid-state reactions.[3,6,14] It removes the uncertainty in synthesis schedules that otherwise bedevils separate measurements and at the same time shores up the underdeterminancy of techniques deployed singly. This paper concerns the synthesis of cadmium oxide from a hydroxyl gel for which combinations of XRD, XAFS, and SAXS afford a comprehensive in situ picture of the development of the crystallography, the local atomic structure, and the microstructure. The synthesis of cadmium oxide employed here also forms an efficient mechanism for introducing cadmium oxide (and other divalent oxide) nanoparticles into zeolitic hosts.[15,16] In tracking the detailed crystallography, local atomic structure, and microstructure of these stuffed microporous systems, we have utilized the same portfolio of X-ray techniques,[17] for which the present study following the thermal synthesis of cadmium oxide from a hydroxyl gel forms the foundation.

Experimental Section

Specimen Preparation. The cadmium hydroxide gel was prepared by mixing 0.1 M cadmium acetate with 0.1 M sodium hydroxide. The mixture was continuously stirred for 4 h at room temperature and then washed and filtered. The recovered hydroxyl gel was then heated at 90 °C for 12 h, which resulted in a white dispersed powder. This was the starting material for the in situ combined X-ray experiments. Ex situ XRD powder patterns using Cu Kα from a rotating anode source were also obtained, both on the hydroxyl gel and after heating at 500 °C for 1 h.

Combined X-ray Experiments. In situ combined XAFS/XRD experiments using a rapidly scanning monochromator were obtained on station 9.3[3,9,14] at the Synchrotron Radiation Source (SRS) at Daresbury Laboratory and fixed wavelength (1.54 Å) SAXS on station 8.2.[6,11,13] Details of the experimental arrangements can be found in the accompanying references. Specimens of the cadmium hydroxide gel were fabricated as pressed 13 mm disks (under 3 tonnes of pressure) with thicknesses to provide an absorbance of ∼2 at the cadmium K-edge (0.4641 Å) for XAFS/XRD and at 1.54 Å for SAXS. XAFS/XRD scans on station 9.3 were completed every 10 min: 380 s for XRD, 180 s for Cd XAFS, and 40 s dead time for slewing the monochromator.[18] Powder patterns were collected at 1.0456 Å to avoid cadmium fluorescence and XAFS scans extended 600 eV above the K-edge at 26.711 keV. SAXS was measured on station 8.2 with a data collection time of 2 min. An INEL curved position-sensitive detector was used for XRD on station 9.3. Specimen heating on both stations was conducted in a nitrogen atmosphere for SAXS and in air for XAFS/XRD using a purpose-built furnace.[19] The specimen temperature was raised from room temperature to 600 °C at 10 °C min^{-1} for SAXS experiments and at 5 °C min^{-1} for combined XAFS/XRD experiments.

Results

Ex situ powder patterns of the cadmium hydroxide starting material and that resulting from heating this at 500 °C are shown in parts a and b of Figure 1, respectively. The lines were indexed using the published structures for $Cd(OH)_2$[20] for Figure 1a and

[†] University of Wales.
[‡] The Royal Institution of Great Britain.

10.1021/jp984091m CCC: $18.00
Published on Web 04/10/1999

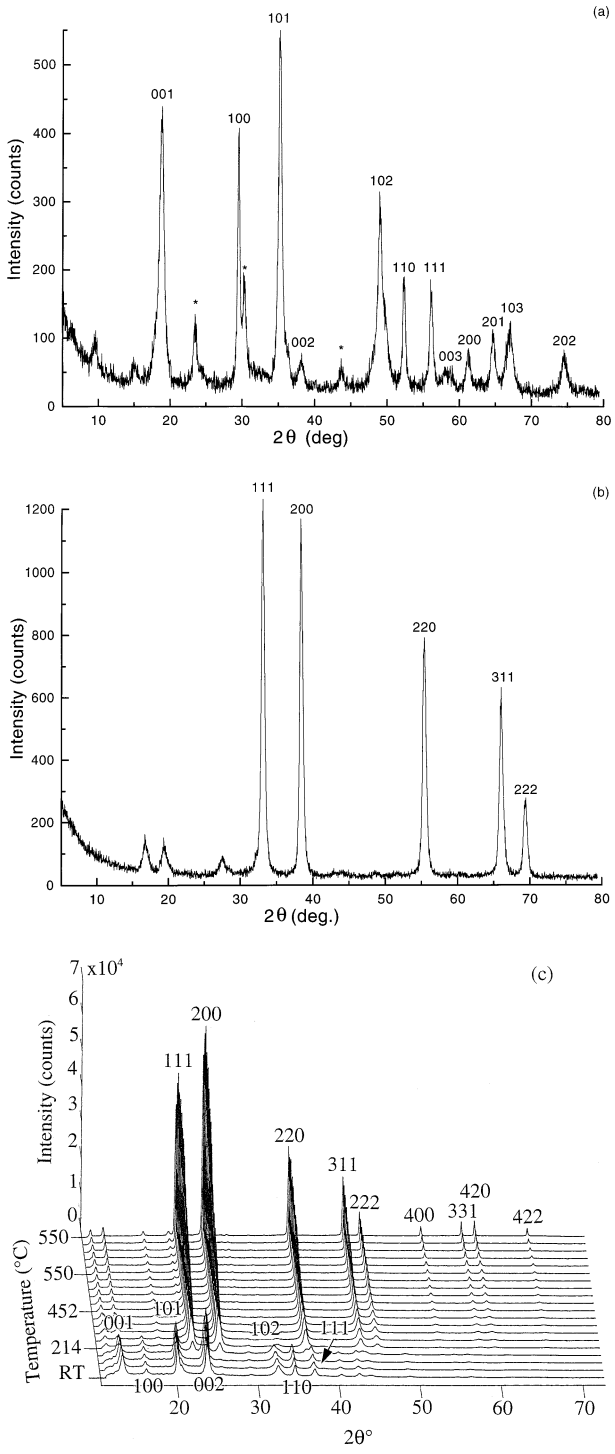

Figure 1. XRD powder patterns for the hydroxyl starting material (a) and the converted oxide, following heat treatment for 1 h at 500 °C (b). Both were measured ex situ using a Cu Kα (1.54 Å) rotating anode source. The indexing of lines is taken from the structure of $Cd(OH)_2$[20] for (a) and CdO[21] for (b). The lines marked * are identified as residual otavite ($CdCO_3$). In situ XRD (1.0456 Å) following the synthesis of cadmium oxide is shown in (c). The stacked plots are at 50 °C intervals, each of 10 min.

CdO[21] for Figure 1b. A small quantity of otavite ($CdCO_3$) can also be identified in Figure 1a. In situ XRD scans following the synthesis of CdO are shown in Figure 1c, the conversion taking place close to 182 °C, although CdO is first noticed at 120 °C. This can be seen clearly in Figure 2a where the integrated peak areas for $Cd(OH)_2$ (101) and CdO (111) reflections are shown. The peak widths (full width at half-maximum, fwhm) for both reflections are shown in Figure 2b, and although these are initially comparatively broad, the CdO (111) reflection narrows substantially between 180 and 550 °C, indicating increasing crystallite size. In situ cadmium XAFS was measured in conjunction with the XRD. The corresponding Fourier transforms obtained from spectra at room temperature and at 550 °C are shown in parts a and b of Figure 3, respectively, revealing the different real space local structure around cadmium in the hydroxide compared to the oxide. In situ SAXS data are plotted in Figure 4 as $I(q)$ versus q (a) and as ln $I(q)$ versus ln q (b), where q is the scattering vector. It is clear from a comparison of Figure 4a with Figure 2a that there is a reduction in scattering around the onset of cadmium oxide, ~120 °C, which then grows, rising to a maximum ~350 °C and eventually falling away as the conversion is completed around 550 °C. From the ln−ln plots in Figure 4b, it is evident that there are substantial linear regions at the start and at the end but that in between a kink appears which moves progressively to lower q as the synthesis advances.

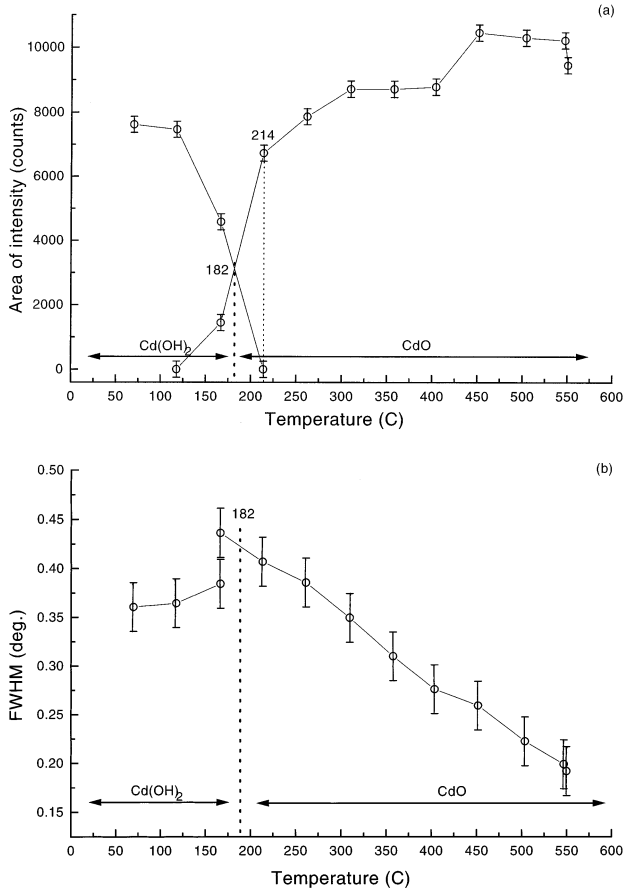

Figure 2. Progression of synthesis from XRD: integrated peak areas from Figure 1c for $Cd(OH)_2$ (101) and CdO (111) reflections (a) with fwhm line widths plotted in (b). The line widths are used to obtain the crystallite particle sizes L_{XRD} plotted in Figure 5a where they can be compared with independent estimates from the positions of the kinks in the SAXS plots (Figure 4b).

Analysis and Discussion

XRD. In Figure 2a it can be seen that the growth of the cadmium oxide phase judged from the integrated XRD peak area continues beyond 214 °C, after the source of cadmium hydroxide has ceased. This suggests the existence of either an amorphous or a nanocrystalline cadmium oxide phase. While there is some residual diffuse scattering in in situ patterns for the starting hydroxide material (Figure 1c), this component

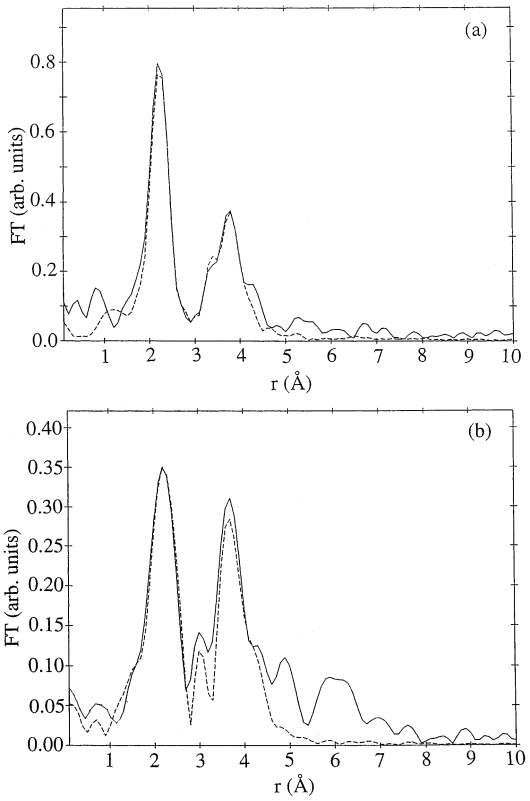

Figure 3. Results of Cd K-edge XAFS measured in situ at 20 °C (a) and 550 °C (b). The Fourier transforms of weighted normalized fine structure (χk^3) are shown plotted as a function of the interatomic distance from cadmium. (k is the photoelectron wavevector, $[2m_e(E - E_0)]^{1/2}/\hbar$, where E is the X-ray energy and E_0 the position of the absorption edge threshold). Solid lines are experimental results, and dotted lines are the result of least-squares analysis fitting χk^3 using EXCURV92 ($E_F = -4$ eV, VPI = 0 and AFAC = 0.8). Results for cadmium local environments obtained from XAFS are listed in Table 1 where they are compared to the crystallographically determined local structures. The changing of the Cd−O Debye−Waller factor, $2\sigma^2$, with temperature throughout the heat treatment for (a) and (b) and for intermediate spectra is plotted in Figure 5b.

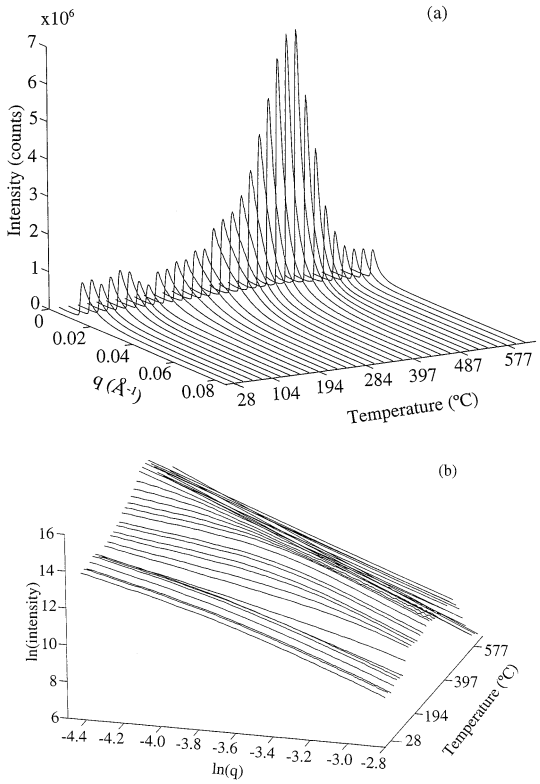

Figure 4. In situ SAXS following the synthesis of cadmium oxide from a hydroxyl gel: $I(q)$ vs q (a) and ln $I(q)$ vs ln q (b). The SAXS camera length was 3.5 m and provided a wave vector window ($q = 4\pi\sin\theta/\lambda$) of 0.000 25 to 0.0844 Å^{-1}. SAXS profiles are given at temperature intervals of ~20 °C and time intervals of 2 min. Crystallite particle sizes L_{SAXS} obtained from the kinks in (b) are given in Figure 5a and the SAXS invariant in Figure 5c.

virtually disappears beyond 200 °C, pointing to the existence of cadmium oxide nanocrystals too small to register in the measured integrated (111) peak area. By use of the Scherrer equation[22] and assuming that the particles are spherical, the particle size L_{XRD} that contributes to the measured the line width $\Delta\theta$ for a given wavelength λ is given by

$$L_{XRD} = \frac{K\lambda}{\Delta(2\theta)\cos\theta}$$

where θ is the Bragg angle for the reflection and K is a constant that is approximately unity. Taking the line widths plotted in Figure 2b, the corresponding crystallite sizes for cadmium oxide start around 125 Å at 160 °C, more than doubling by 550 °C, as shown in Figure 5a. The continued growth of the cadmium oxide phase beyond 214 °C presumably stems from the presence of much smaller particles, which add to the wings of the diffraction peak.

In Figure 6 the XRD particle volume ($\pi L_{XRD}^3/6$) is compared at different stages during the synthesis to the (111) peak area, which measures the growth of the cadmium oxide phase. The relationship is far from linear, with no significant increase in crystallite volume until the initial stage of growth is complete around 350 °C. The existence of smaller crystallites in this regime would not radically alter this or the dramatic increase in the later stages of growth between 350 and 550 °C. This behavior is symptomatic of dendritic growth followed by Ostwald ripening, as indicated in Figure 6. Accordingly, we expect microstructure with fractal character for the initial cadmium oxide product formed below 350 °C.

XAFS. The dotted curves shown for the selected Fourier transforms in Figure 3 are the outcome of least-squares analysis of the weighted spectra, resulting in the local structures for cadmium listed in Table 1. This also includes the crystallographic environments for $Cd(OH)_2$[20] and CdO[21] with which the present XAFS determinations are in good agreement. Note that from room temperature to 550 °C the nearest-neighbor oxygen shell distance r_{Cd-O} increases by 0.03 Å while that of the first shell of cadmiums r_{Cd-Cd} decreases by 0.18 Å. Analysis of intermediate spectra reveals that these two interatomic distances that differentiate the hydroxide from the oxide crystalline structures both switch between 160 C and 200 °C, in good agreement with the conversion between these two phases recorded by in situ XRD (Figure 2a). Table 1 also reveals how the XAFS Debye−Waller factor σ^2_{Cd-O}, which measures the variance in r_{Cd-O}, increases significantly for the nearest-neighbor octahedron of oxygens from room-temperature cadmium hydroxide to cadmium oxide at 550 °C. Since there is no reported structural disorder in this shell of oxygens in either phase,[20,21] the increase must be thermal in origin. The analyzed values of σ_{Cd-O}^2 obtained from in situ XAFS/XRD experiments are plotted in Figure 5b, where an approximately linear dependence on temperature is obtained. The small shoulder around 182 °C can be attributed to the difference in oxygen nearest-neighbor distances between $Cd(OH)_2$ and CdO ($(2 \times 0.03)^2 \approx 0.002$ Å^2).

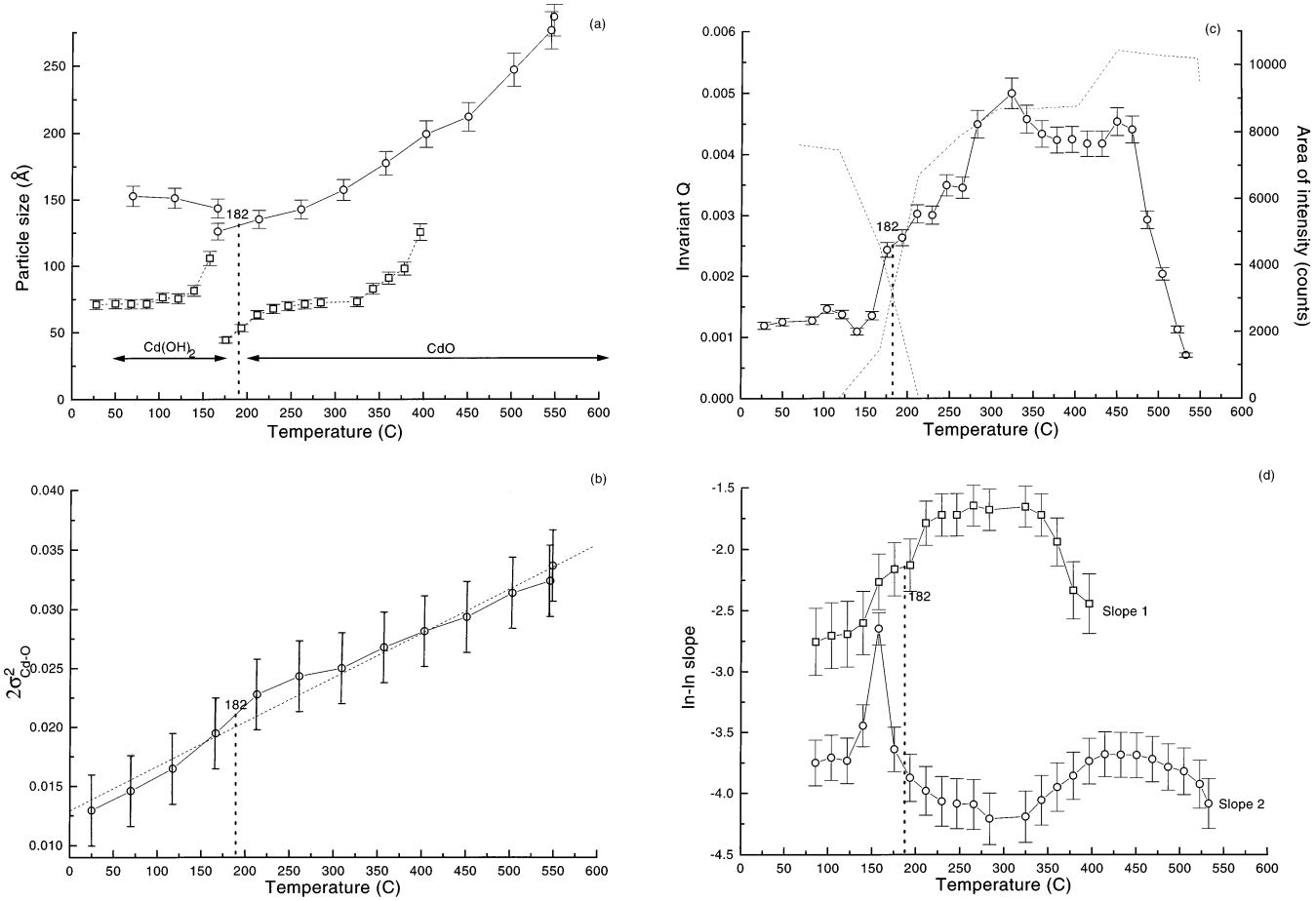

Figure 5. (a) Crystallite size L_{XRD} plotted as a function of temperature and derived using the Scherrer equation employing the in situ XRD line widths taken from Figure 2b, (101) for $Cd(OH)_2$ and (111) for CdO. The dashed lines are the corresponding values of L_{SAXS} obtained from the change in slope of the in situ SAXS profiles from Figure 4b. (b) XAFS Debye−Waller factor σ_{Cd-O}^2 analyzed from the in situ XAFS spectra as a function of specimen temperature. The linear dependence on temperature is in agreement with the Einstein model from which a Cd−O stretching frequency of 291 cm^{-1} is obtained. (Note anharmonicity terms were not significant in the EXCURV92 analysis over these temperatures.) (c) Course of the in situ SAXS invariant Q throughout the synthesis. The growth and decay of phases from Figure 2a are superimposed. (d) Slopes from Figure 4b, the lower indicative of surface scattering mainly from smooth particles, the higher pointing to a fractal structure for temperatures between 150 and 400 °C. See text for details.

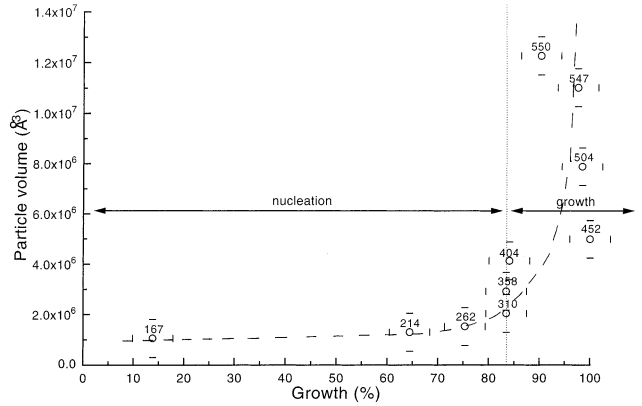

Figure 6. Crystalline growth and crystallite volume ($\pi L_{XRD}^3/6$) compared for cadmium oxide taken from the in situ XRD data given in Figure 2a and Figure 5a, respectively; see text for details. The initially flat regime for the crystallite volume can be interpreted as dendritic nucleation, with the sharp rise above 350 °C being associated with Ostwald ripening, a picture substantiated by the broad peak in the SAXS invariant (Figure 5c) and the fractal nature of bulk scattering slope (Figure 5d).

The contribution to XAFS Debye−Waller factors due to thermal motion can be estimated from the Einstein model, modified by replacing the independent frequency of single atoms by the correlated frequency of pairs of atoms. This phenomenological approach offers very satisfactory agreement with empirical values for simple halides and metals.[23] In particular, if ω_{Cd-O} is the stretching frequency of nearest neighbors and μ is the reduced mass of the absorber and backscatterer and if the temperature exceeds the Einstein temperature $h\omega_E/k$, then the amplitude of Cd−O vibrations is given by the classical relationship

$$\sigma_{Cd-O}{}^2 = \frac{kT}{\mu\omega_E{}^2}$$

When this is applied to Figure 5b, the slope yields a frequency of 291 cm^{-1} for Cd−O vibrations. We note that the IR band for Cd−O vibrations in phosphate and borate glasses, for instance, occurs at 150 cm^{-1}, increasing to 200 cm^{-1} with cadmium concentration,[24,25] so we might expect an even higher figure for Cd−O vibrations in $Cd(OH)_2$ or CdO.

SAXS. The invariant Q measures the electron density contrast ($\Delta\rho$) independent of particle shape or number. For a simple two-phase system[26]

$$Q \propto \int_0^\infty Iq^2\,dq \propto \phi(1-\phi)\Delta\rho^2$$

where ϕ is the fraction of one phase and a maximum is predicted

TABLE 1: Environments of Cadmium in $Cd(OH)_2$[20] and CdO:[21] X-ray Diffraction and in Situ XAFS Compared

	XRD[20,21]			XAFS (this study)			
phase	CN	atom type	interatomic distance r_{Cd-X} (Å)	CN	atom type	interatomic distance r_{Cd-X} (Å)	Debye−Waller factor σ_{Cd-X}^2 (Å)^2
$Cd(OH)_2$, rt	6	O	2.315	6	O	2.27	0.013
	6	Cd	3.496	6	Cd	3.50	0.019
	6	O	4.100	12	O	4.02	0.070
	6	O	4.193				
CdO, 550 °C	6	O	2.348	6	O	2.30	0.032
	12	Cd	3.320	12	Cd	3.32	0.042
	8	O	4.066	8	O	4.11	0.030

when ϕ (and therefore $(1 - \phi)$, the fraction of the other phase) is 50%. Replacing ${}_0\int^\infty$ by ${}_{q_{min}}\int^{q_{max}}$ for the q range employed here (0.00025−0.0844 Å^{-1}) typically removes a small constant but does not affect the overall shape.[27] Q for the in situ SAXS profiles is plotted in Figure 5c. The decline of cadmium hydroxide and the growth of cadmium oxide from in situ XRD (Figure 2a) are superimposed for comparison. The main rise in Q occurs around 160 °C, following the initial fall in the cadmium hydroxide phase, and reflects a mixture of both hydroxide and oxide whose densities are not identical. Q, however, continues to grow beyond the disappearance of cadmium hydroxide. As we have suggested, XRD points to the existence of smaller cadmium oxide particles, but these will offer little contrast in $\Delta\rho$ for SAXS. Nevertheless, Q reaches a significant maximum around 325 °C and then commences to fall, reaching its lowest value by 550 °C. This broad peak in Q coincides with the cadmium oxide regime and most probably relates to changes in the physical dispersion of crystallites, the SAXS contrast coming from entrapped gas (nitrogen) and eventually disappearing with densification. As we have seen in Figure 6, growth of the cadmium oxide phase occurs without much change in crystallite volume at temperatures below 350 °C, the major growth in particle volume taking place above 350 °C. Accordingly, the peak in Q at ∼325 °C in Figure 5c can be interpreted as the point at which approximately half the specimen volume is taken up by included nitrogen and the remainder by nanocrystalline cadmium oxide.

A similar picture emerges from considering the q dependence of the scattered intensity $I(q)$, evident in the linearity of the ln−ln plots illustrated in Figure 4b. The kinks referred to earlier mark a change in slope, initially at ∼70 °C, from about −3 to about −4, indicative of bulk scattering[28] and Porod (or surface) scattering,[29] respectively. If L_{SAXS} is the particle size to which SAXS is sensitive, the changeover from bulk to surface scattering occurs where $qR_g \approx 1$. Values of L_{SAXS} $(=2R_g)$ obtained from in situ SAXS are also plotted in Figure 5a. Falling between 50 and 100 Å, these are approximately half those of the corresponding L_{XRD}, but L_{SAXS} tends to L_{XRD} as the temperature approaches either 182 or 400 °C. The relevant q range, which is primarily measured in the SAXS tail, is more sensitive to smaller particle sizes compared to the XRD fwhm measurements. Accordingly, Figure 5a gives an indication of the dispersity of cadmium hydroxide particle sizes below 182 °C and of cadmium oxide particle sizes up to 400 °C.

Finally, the $\ln I(q)$ versus $\ln q$ slopes above and below the kink are plotted in Figure 5d. With one exception the slope at high q stays around −4, suggesting cadmium hydroxide and cadmium oxide particles irrespective of size are reasonably smooth. Around 150 °C, where the first XRD evidence for cadmium oxide emerges, there is a momentary increase in slope from −4 to −3, suggesting cadmium hydroxide particles are roughening in the initial conversion to cadmium oxide. By contrast, the slope at low q also rises at this point, continuing to rise with temperature and eventually falling when the volume of cadmium oxide particles begins to increase dramatically (Figure 6) as densification sets in. Slopes in this intermediate region of about −2 in Figure 5d point to a fractal geometry consistent with the dendritic growth mechanism proposed earlier in the interpretation of Figure 6.

Precipitating CdO in Zeolitic Hosts. Synthesizing cadmium oxide nanoparticles within zeolitic hosts has been described by Wark and co-workers.[15,16] Cadmium acetate is used to introduce cadmium into zeolite structures by ion exchange. Treatment with NaOH followed by calcination at 500 °C results in the occurrence of particles of cadmium oxide, which, on the basis of optical measurements and electron microscopy, are estimated to be 1−2 nm in size entrapped in Na−zeolite Y.[15] Using in situ XAFS, XRD, and SAXS in conjunction with UV−vis spectrometry, we have been able to confirm the atomic and microstructural basis for these conclusions.[17]

Summary

In the present study the synthesis of cadmium oxide from a gel of cadmium hydroxide nanoparticles has been followed in situ and in considerable structural detail using the advantageous combination of XRD, XAFS, and SAXS. In situ XRD and cadmium XAFS reveal that the transformation of the hydroxide into the oxide occurs at 182 °C. From the XRD line widths the volume of cadmium oxide nanocrystals remains practically constant up to 325 °C, indicative of nucleation. Major particle growth then ensues as the temperature rises toward 550 °C. Over the same temperature history considerable changes occur in the microstructure, with a sizable rise in the SAXS invariant Q occurring between 140 and 325 °C spanning the nucleation of CdO particles and pointing to included gas. Thereafter, Q falls to a minimum by 550 °C, characteristic of a monophasic microstructure. Over the course of the solid-state reaction of cadmium hydroxide into cadmium oxide, $\ln(I(q))$ versus $\ln(q)$ plots exhibit two slopes, indicative of bulk and surface scattering from nanosize crystallites, where the changing particle dimension (50−100 Å) correlates with the estimates from XRD fwhm values. The bulk scattering and Porod slopes at the start and end of the synthesis are indicative of three-dimensional aggregates of smooth particles. During nucleation though, changes in the bulk scattering slope reflect a transient low-dimensional microstructure, pointing to a dendritic mechanism. As growth takes hold, the slope decreases in concert with Q, indicating that densification is complete. Detailed knowledge of the nucleation and growth of cadmium oxide precipitated unimpeded from a hydroxide gel is proving to be critical in distinguishing parallel processes in zeolitic hosts where growth is restricted by microporous containment.

Acknowledgment. We thank Professors C. R. A. Catlow and J. M. Thomas for their help and encouragement, Drs. A. J. Dent and E. Komanschek for experimental assistance, and Dr. G. D. Chryssikos for helpful discussions. Oxford Instruments is thanked for the provision of a studentship (C.A.) and EPSRC for making synchrotron radiation facilities available at the Synchrotron Radiation Source at CLRC's Daresbury Laboratory. Finally, we take this opportunity to congratulate Professor Austen Angell on reaching 65 and to salute his trail-blazing dedication in confronting and taming complexity in glasses, polymers, and liquids alike.

References and Notes

(1) Brinker, C. J.; Scherer, G. W. In *Sol−Gel Science*; Academic Press: San Diego, 1990.
(2) Gleiter, H. *Adv. Mater.* **1992**, *4*, 474.
(3) Colyer, L. M.; Greaves, G. N.; Carr, S. W.; Fox, K. K. *J. Phys. Chem. B* **1997**, *111*, 10105.
(4) Herron, N.; Wang, Y.; Eddy, M. M.; Stucky, G. D.; Cox, D. E.; Moller, K.; Bein, T. *J. Am. Chem. Soc.* **1989**, *111*, 530.
(5) Chadwick, A. V.; Russel,N. V.; Whitham, A. R.; Wilson, A. *Sens. Actuators* **1994**, *18−19*, 99.
(6) Oversluizen, M.; Bras, W.; Greaves, G. N.; Clark, S. M.; Thomas, J. M.; Sankar, G.; Tiley, B. *Nucl. Instrum. Methods Phys. Res., Sect. B* **1995**, *97*, 184.
(7) Craievich, A. F.; Santilli, C. V.; Pulcinelli, S. H, *Nucl. Instrum. Methods Phys. Res., Sect. B* **1995**, *97*, 78.
(8) Dieudonné, Ph.; Delford, P.; Phalippou, J. *J. Non-Cryst. Solids* **1998**, *225*, 220.
(9) Sankar, G.; Wright, P. A.; Natarajan, S.; Thomas, J. M.; Greaves, G. N.; Dent, A. J.; Dobson, B. R.; Ramsdale, C. A.; Jones, R. H. *J. Phys. Chem.* **1993**, *97*, 9550.
(10) Couves, J. W.; Thomas, J. M.; Waller, D.; Jones, R. H.; Dent, A. J.; Derbyshire, G. E.; Greaves, G. N. *Nature* **1991**, *354*, 465.
(11) Bras, W.; Derbyshire, G. E.; Ryan, A. J.; Mant, G. R.; Felton, A.; Lewis, R. A.; Hall, C. J.; Greaves, G. N. *Nucl. Instrum. Methods Phys. Res., Sect. A* **1993**, *326*, 587.
(12) Clausen, B. S.; Graback, K.; Steffensen, G.; Hansen, P. L.; Topsøe, H. *Catal. Lett.* **1993**, *20*, 23.
(13) Fernades, J. C.; Hall, D. A.; Greaves, G. N. *Mater. Sci. Forum* **1998**, *228−231*, 411.
(14) Thomas, J. M. T.; Greaves, G. N. *Science* **1994**, *265*, 1675.
(15) Tkachenko, O. P.; Shpiro, E. S.; Wark, M.; Schulz-Ekloff, G.; Jaeger, N. I. *J. Chem. Soc., Faraday Trans.* **1993**, *89*, 3987.
(16) Khouchaf, L.; Tuilier, M. H.; Wark, M.; Paillaud, J. J.; Soulard, M. *J. Phys. IV (France)* **1997**, *7*, c2−c267.
(17) Greaves, G. N.; Alétru, C.; Colyer, L.; Sankar, G. *Jpn. J. Appl. Phys.*, in press.
(18) Dobson, B. R. *Synchrotron Radiat. News* **1994**, *11*, 21.
(19) Dent, A. J.; Dobson, B. R.; Greaves, G. N.; Sankar, G.; Roberts, M.; Catlow, C. R. A.; Thomas, J. M., *Physica B* **1995**, *208*, 2523.
(20) Bertrand, G.; Dusausoy, Y. *C. R. Hebd. Seances ′Acad. Sci., Ser. C* **1970**, *270*, 612.
(21) Cimino, A.; Marezio, M. *J. Phys. Chem. Solids*, **1960**, *17*, 57.
(22) Klug, H. P.; Alexander, L. P. In *X-ray Diffraction Procedures*; Wiley: New York, 1974.
(23) Frenkel, A. I.; Stern, E. A.; Newville, M. *Phys. Rev. B* **1993**, *48*, 12449.
(24) Walrafen, G. E.; Revesz, A. G. In *Structure and Bonding in Non-Crystalline Solids*; Plenum: New York, 1986; p 203.
(25) Kamitsos, E. I.; Chryssikos, G. D. *J. Non-Cryst. Solids* **1987**, *63*, 611.
(26) Srobl, G. R.; Schneider, M. J. *J. Polym. Sci., Part B: Polym. Phys.* **1981**, *19*, 1361.
(27) Ryan, A. J.; Bras, W.; Derbyshire, G. E.; Mant, G. R. *Polymer* **1994**, *35*, 4537.
(28) Schaefer, D. W. *Science* **1989**, *243*, 1023.
(29) Guinier, A. *Ann. Phys.* **1939**, *12*, 161.